International Journal of Heat and Mass Transfer 187 (2022) 122511

Contents lists available at ScienceDirect

International Journal of Heat and Mass Transfer

journal homepage: www.elsevier.com/locate/hmt

Two-layer transient heat transfer using impulse response methods

Shawn Siroka*, Reid A. Berdanier, Karen A. Thole

The Pennsylvania State University, 3127 Research Drive, State College, PA 16801, USA

ARTICLE INFO

Article history:
Received 6 August 2021
Revised 26 November 2021
Accepted 29 December 2021

ABSTRACT

Solutions to the inverse heat conduction problem (IHCP) are methods that can be used to quantify surface heat flux in multi-layer materials for components in which there are limited subsurface (internal) temperature measurements, such as coated components. A critical consideration is to capture high frequency fluctuations using a practical heat flux sensor. To that end, this paper highlights key parameters for calculating accurate surface heat transfer. Specifically, this research extends the available solutions to the IHCP for multi-substrate structures through an impulse response methodology. The sensitivity of the impulse method was quantified with respect to practical measurements. When compared to the inverse case, the impulse method resulted in lower errors when calculating surface heat flux over a range of conditions. Overall, this work provides a foundation for deducing heat flux from a subsurface heat flux sensor while maintaining a high-frequency response.

1. Introduction

Quantifying heat flux in hot components is critical to achieving desired part life. One common method for measuring heat flux is the use of differential temperature gauges (HFGs) [1]. These sensors comprise two temperature measurements at known locations on opposing sides of a substrate with known thermal and geometric properties. As an extension, transient heat flux is calculated at the surface by solving the unsteady conduction equation using the two temperature measurements and the properties of the inner substrate. However, the location of the temperature in a layered measurement sensor affects the operation and the processing required to solve for the transient heat transfer. For instance, if one of the temperature sensors is on the surface of the component itself, the boundary conditions for the conduction equation are known and the surface heat flux can be calculated directly; this example is considered a direct problem. Direct problems have been solved through a number of techniques [2–4], but one of the most computationally efficient methods is through the use of an impulse response filter. Oldfield [2] employed the impulse technique to deduce surface heat flux from temperature measurements on opposing sides of a substrate and found numerical errors of less than 0.014%.

In contrast to direct problems, indirect problems use one or multiple subsurface temperatures to calculate surface heat flux. The indirect problem requires a different processing analyses because the conduction equation is ill-posed. The ill-posed nature of the conduction equation is because surface conditions are damped as thermal energy propagates through the subsequent layers to the measurement location of a multi-layer part. Because of the damping, internal measurements must be rectified to obtain the values at the surface. Inverse solution methods are a vast arena of mathematics [5,6] with several applications [7,8]. The work presented here specifically focuses on solutions to the inverse heat conduction problem (IHCP).

Several techniques have been used to solve the IHCP for a single-layer system. Broadly, these solutions can be split into entire-domain numerical solutions [9] and filter-based solutions [10,11]. The entire-domain approaches use either analytical solutions to conduction equations [9] or commercial FEA solvers [12] to calculate domain-wide conditions from the internal temperature measurements. This IHCP approach is computationally intensive and cannot be used for real-time processing [11]. On the other hand, filter-based solutions are computationally efficient and can be used for real-time processing. Therefore, this methodology is an ideal choice for applications requiring integrated feedback for controls.

Within the architecture of filter-based solutions, approaches based on Green's Function [10,13] have been commonly used to solve single-layer domains, and machine learning algorithms have also been explored [14]. However, few studies have extended these techniques to composite structures, which are central to many real-world applications, such as coated systems. Najafi et al. [15] provides one such filter-solution to the two-

* Corresponding author.
E-mail address: sis5702@psu.edu (S. Siroka).

https://doi.org/10.1016/j.ijheatmasstransfer.2021.122511
0017-9310/

Nomenclature

A	convenience variable
c	specific heat
d	thickness
f	frequency $= 0.5\ \omega\pi^{-1}$
h	impulse response coefficient
j	imaginary number $= \sqrt{-1}$
k	thermal conductivity
n	any integer
q	heat flux
Q	surface heat flux related to a boundary condition
t	time
t^*	nondimensional time
x	spatial variable
X	arbitrary variable
Z	imaginary wave number

Greek

α	thermal diffusivity $= \mathrm{kc}^{-1}\rho^{-1}$
ϵ	error in quantity
λ	thermal penetration wave length $\sqrt{2\alpha\omega^{-1}}$
ρ	density
σ	ratio of thermal effusivities
Φ	phase
ω	angular frequency $= 2\pi\mathrm{f}$

Subscripts and accents

0	related to the surface condition
1	related to the first temperature device
2	related to the second temperature device
amp	related to the amplitude
an	related to the analytical solution
c	related to the coating
com	related to the computational solution
cut	cutoff
phase	related to the phase
s	related to substrate
$\bar{a}$	mean/DC quantity
$\bar{a}$	fluctuating/AC quantity
$\bar{a}$	amplitude of AC quantity

layered IHCP based on a domain splitting technique to formulate a computationally-efficient transformation filter using a sum-of-square error minimization with a Tikhonov regularization (TR) to stabilize the solution. Their solution showed small numerical errors for a variety of cases. The Najafi et al. solution currently serves as the only filter-based composite solution in open literature. Unfortunately, this solution employs a regularization scheme that requires a priori information about the problem for correct selection of the regularization parameter [16]. This drawback can be bypassed through the use of an impulse response approach, which is described in this paper.

The processes contained within this work are general to any 1D multi-layer linear time-invariant system with a focus on two-layer systems for their practicality. Often, temperature sensors are coated to increase sensor robustness or embedded at various depths of a material with a thermal gradient. The guidelines presented throughout this paper provide insight to deduction of heat flux from such sensors and the design of novel heat flux gauges where a tradeoff between durability and sensor response time exists. Another purpose of this study is to add to the number of solutions for composite IHCP systems by extending the impulse response direct method presented by Oldfield [2] to an indirect two-layer 1D transient system. This innovative processing scheme for

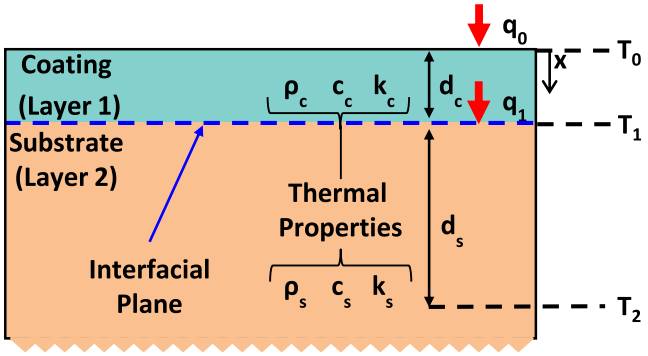

Fig. 1. Two-layer (coating and substrate) domain with important locations highlighted.

multi-layer one-dimensional thermal components provides a suitable alternative for existing methods without the introduction of a regularization parameter. To accomplish these goals, this paper first provides a detailed outline of design considerations for transient two-layered heat transfer. Next, this work compares the proposed impulse response method with the traditional inverse processing method by Najafi et al. [15]. Finally, the sensitivity of the impulse response method is characterized in terms of thermal property errors and signal noise.

1.1. Methodology of composite inverse problems

The methodology of inverse problems is complex. Therefore, it is important to provide guidelines on when such processes are necessary and how those processes can be deployed. This section first discusses the practical considerations on when a coating layer starts to affect heat transfer measurements. Then, this section discusses two processing options to correct for the coating layer in the case of two-layer systems that contain two internal temperature measurements.

1.2. Considerations of two-layer heat transfer gauges

The methods presented in this paper are general to any multi-layer one-dimensional, linear, time-invariant component. However, as a new contribution, this paper explores a two-layer application. Fig. 1 illustrates the domain, which serves as the basis for the rest of the analyses. The two distinct domain regions are labeled as Layer 1 and Layer 2, but are characterized in the context of a coated component. For that reason, domain quantities are denoted with a "c" subscript for the coating layer (Layer 1) and a "s" subscript for the substrate layer (Layer 2). Within Fig. 1, a few key planes are highlighted and denoted including: surface quantities such as temperature (T_0) and heat flux (q_0) that are denoted with a zero subscript; the interface sensor location that is denoted with a subscript of one (T_1, q_1) at a distance related to the thickness of the coating (d_c); the location of the second internal temperature sensor is denoted with a subscript of two (T_2), and its location is defined by the combined thickness of the coating and substrate layers ($d_c + d_s$).

The coating layer is a thermal damper to the underlying measurement planes, which imposes limitations resulting from the dissipation of thermal energy upstream of the measurement location. One method to quantify this damping is to analyze the temperature response to a steady harmonic surface heat flux. Eq. (1) and Eq. (2) show the governing equations for both domains where the temperature solution through the coating and substrate are $T_c(x,t)$

Table 1
Boundary conditions for harmonic surface heat flux.

Boundary Conditions	
$q_0 = \hat{Q}\cos(\omega t)$	at $x = 0$
$T_c = T_s$	at $x = d_c$
$k_c \frac{\partial T_c}{\partial x} = k_s \frac{\partial T_s}{\partial x}$	at $x = d_c$
$T_s = 0$	at $x \to \infty$

and $T_s(x,t)$:

$$\frac{\partial^2 T_c}{\partial x^2} = \frac{1}{\alpha_c}\frac{\partial T_c}{\partial t} 0 \le x \le dc \tag{1}$$

and

$$\frac{\partial^2 T_s}{\partial x^2} = \frac{1}{\alpha_s}\frac{\partial T_s}{\partial t} dc \le x < \infty \tag{2}$$

where α_c and α_s are the thermal diffusivity for the coating and substrate.

Table 1 shows the boundary conditions used for the analysis. Because this is a steady-state solution, no initial conditions are necessary to solve the governing differential equations. The solutions were obtained following conventional procedures to steady-state harmonic conduction problems [17]. Previously, part of this solution was published [3], but the current work expands the solution to both layers of the domain, which is more applicable to a coated system approach.

Each layer was solved using a corresponding superposition of real and imaginary solutions. The temperature through the coating (T_c) and through the substrate (T_s) are given as

$$T_c(x,t) = Re\left\{\left(\frac{\hat{Q}}{k_c Z_c}\right)\frac{(1+\sigma)\exp(-Z_c(x-d_c)) + (1-\sigma)\exp(Z_c(x-d_c))}{(1+\sigma)\exp(Z_c d_c) + (1-\sigma)\exp(-Z_c d_c)}\exp(i\omega t)\right\} \tag{3}$$

and

$$T_s(x,t) = Re\left\{\left(\frac{2\hat{Q}}{k_c Z_c}\right)\frac{\exp(-Z_s(x-d_c))}{(1+\sigma)\exp(Z_c d_c) + (1-\sigma)\exp(-Z_c d_c)}\exp(i\omega t)\right\} \tag{4}$$

where the ratio of thermal effusivities (σ) is

$$\sigma = \sqrt{\frac{\rho_s c_s k_s}{\rho_c c_c k_c}} \tag{5}$$

and the imaginary wave numbers (Z) are

$$Z_c = \sqrt{\frac{i\omega}{\alpha_c}} \text{ and } Z_s = \sqrt{\frac{i\omega}{\alpha_s}} \tag{6}$$

with the other necessary quantities defined in Fig. 1.

The solution in Eq. (3) can be particularly useful to assess the design space and limitations of two-layer HFGs over a range of frequencies. Fig. 2 serves as an example of the solution to the two-layer harmonic heat flux equation solved using the quantities found in Table 2. Fig. 2(a) shows the harmonic heat flux boundary condition at an example driving frequency of 8000 [Hz] with an amplitude of 1×10^4 [Wm^{-2}] across a range of 2 periods. Fig. 2(b) illustrates the temperature fluctuations at the previously highlighted locations across the same range of periods.

Table 2
Geometric and thermal parameters necessary to solve the harmonic heat conduction equation.

Parameter	Value	Units
α_c	8.67E-8	[$m^2\ s^{-1}$]
k_c	0.12	[$W\ m^{-1}\ K^{-1}$]
d_c	1E-6	[m]
α_s	1.44E-7	[$m^2\ s^{-1}$]
σ	1.23	[–]
d_s	5E-5	[m]
ω	16000π	[rad s^{-1}]
$\hat{Q}$	1E4	[Wm^{-2}]
$\bar{Q}$	0	[Wm^{-2}]

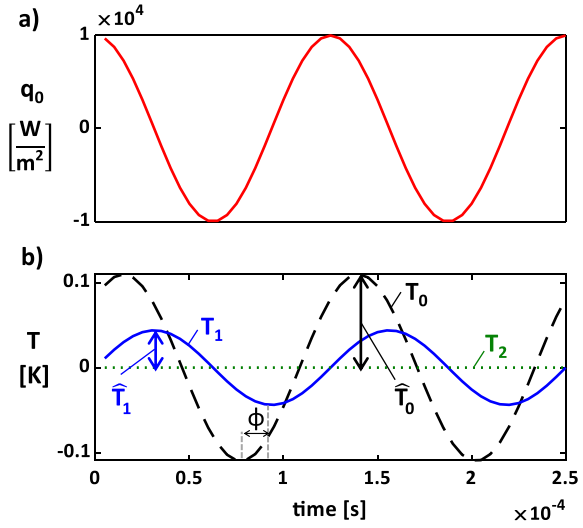

Fig. 2. (a) Harmonic heat flux surface boundary condition and (b) solution to the two-layer harmonic heat conduction equation at selected locations.

Several important characteristics in Fig. 2 illustrate the necessary processing corrections to obtain surface conditions. First, as shown in Fig. 2(b), the peak amplitude of the temperature ($\hat{T}$) decreases significantly from the surface through the coating and substrate. Compared to the T_0 amplitude, the T_1 amplitude in Fig. 2(b) is attenuated. In fact, the surface amplitude has become completely damped in T_2 illustrating the loss of information as the temperature wave propagates through the layers. Second, there is a notable phase shift between the T_0 and T_1 case (highlighted in Fig. 2 as φ) as well as a shift from the T_0 and q_0 case. This shift illustrates that the selected processing scheme must be able to rectify both the shifted phase and damped amplitude of the internal temperature traces to determine true surface conditions.

The identified damping effect has practical implications for the design of a heat flux sensor because the temporal heat flux quantification depends upon a measurable temperature oscillation at T_1. One way to understand the design space of the proposed multi-layer sensor is to quantify the measurement plane amplitude ($\widehat{T_1}$) relative to the surface amplitude ($\widehat{T_0}$). Using the solution to Eq. (3) at the surface and the interface, it can be shown that

$$\frac{\widehat{T_1}}{\widehat{T_0}} = \frac{2\exp\left(-\frac{d_c}{\lambda_c}\right)}{\sigma + 1 + \exp\left(-\frac{2d_c}{\lambda_c}\right)(1-\sigma)} \tag{7}$$

where the thermal coating wavelength is defined as

$$\lambda_c = \sqrt{\frac{2\alpha_c}{\omega}} \tag{8}$$

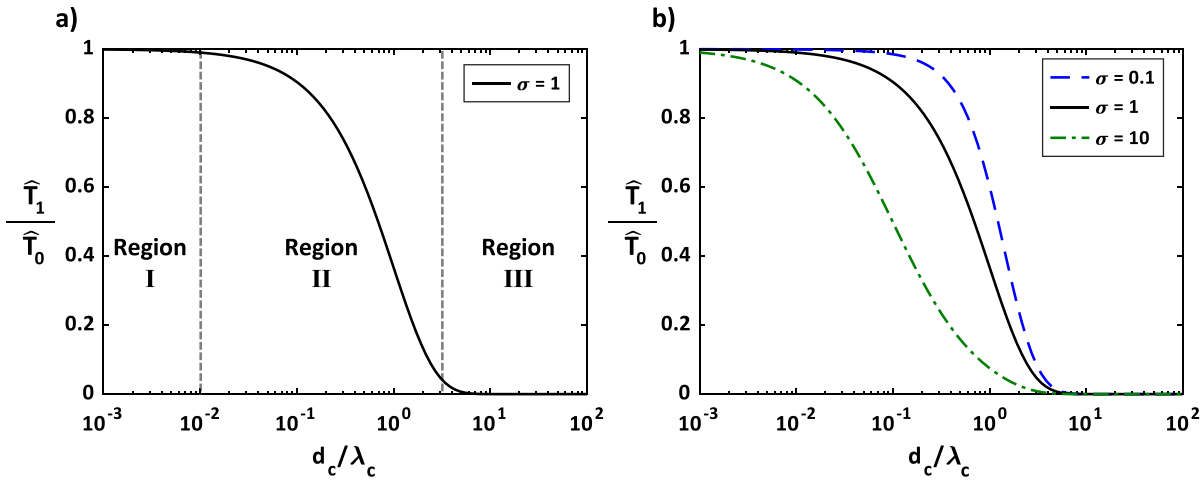

Fig. 3. (a) Ratio of surface temperature amplitude to measurement plane temperature amplitude across a range of non-dimensional coating thicknesses (b) sensitivity of the relative temperature amplitude to the ratio of thermal effusivities.

and where ω is defined as the harmonic heating frequency at the surface.

Eq. (7) illustrates the parameters that are critical to the temperature attenuation at the interface of the layers: the top layer thickness divided by thermal wavelength for the top layer (d_c/λ_c) and the ratio of thermal effusivities for the two layers (σ). Based on these identified dependencies in Eq. (7), the following sections are presented in terms of d_c/λ_c and σ to deduce their physical significance to selected processing schemes.

Fig. 3 plots Eq. (4) for three different σ values across a range of d_c/λ_c conditions displaying the clear design tradeoffs associated with this type of measurement. Fig. 3 provides two key benefits for the ongoing analysis: (i) it graphically shows whether surface conditions can be obtained from the internal temperature points, and (ii) it serves as a guide for the processing steps required to obtain those surface quantities.

Fig. 3(a) can be split into three distinct regions. The first region (I) denotes where the coating can be treated as thermally transparent. Physically, this region represents a coating (Layer 1) with a high thermal diffusivity, a low coating thickness, and a low frequency heat flux. The combination of those characteristics creates a thermally transparent top layer.

Fig. 3(b) illustrates the impact the ratio of thermal effusivities has on this region. The ratio of thermal effusivities (σ) in part dictates how the energy is dissipated between the two domains. Therefore, when the ratio of thermal effusivities is small, more energy will be dissipated in the lower layer, causing the top layer to appear more thermally transparent. It is highly advantageous to develop sensors in this region because the required processing can be simplified to a direct problem. However, it is not always feasible to operate in this region based upon the engineering durability requirements that may be related to the system or the frequency of the heat transfer phenomena of interest.

Region II is defined as the region where the measured temperature amplitude ($\widehat{T_1}$) is substantially attenuated by the coating layer (Layer 1), but not completely damped as illustrated by Fig. 3(a). This region requires indirect processing to rectify the measured temperature to surface conditions. The value of d_c/λ_c that bounds Region II at the lower end depends upon the required accuracy for the application as well as the ratio of thermal effusivities, which is illustrated in Fig. 3(b). However, the upper limit of this region is relatively independent of the ratio of thermal effusivities and can be approximated by a cutoff value of $d_c/\lambda_c = 3$. At that point, the measured signal (T_1) is approximately 5% of the surface temperature and requires extreme amplification to recover the surface conditions for reasonable σ values. High amplification can negatively impact the accuracy of the deduced surface conditions as the signal amplitude approaches the noise floor.

Region III denotes the region where the damping of temperature amplitude through the coating is greater than 95%, meaning there is insufficient information in the measured signal to accurately reproduce the surface conditions. Region III shows the limitations of a two-layer system by defining a strict limit on the phenomena that can be captured. This region also represents the limitations of the indirect methods that will be characterized in subsequent sections, a limit which does not traditionally exist in uncoated systems.

Overall, Fig. 3 illustrates the tradeoffs between coating thermal properties, thickness, and heat flux frequency, while also connecting design decision to the necessary processing procedures. In general, sensors of this type benefit from low σ values up to the point where $d_c/\lambda c = 3$. Furthermore, Fig. 3 provides guidance on whether existing two-layer systems can feasibly use the IHCP solution methods to deduce surface conditions and, if so, where the temperature measurements should be located relative to the surface of interest.

1.3. Indirect methods to obtain surface conditions

The previous section provided guidelines of three different regions in Fig. 3(a): (i) the coating is thermally transparent, (ii) the coating must be accounted for through processing, and (iii) the coating is thermally opaque. To maximize the frequency response or durability of the sensor, it is advantageous to operate in the second region even though it requires more complex (IHCP) processing. The remainder of this paper will focus on solutions for Region 2 while detailing the necessary processing to reconcile damping effects from the coating.

Two different indirect methods were investigated: an inverse method (employing the minimization of the sum-of-the-squared errors between the computed and known values and using TR for stabilizing the solution) and an impulse response method. Both methods assume that the time history from two internal temperature measurements are known and the surface conditions are the desired parameters. Although there are many ways to deduce the surface conditions, these two methods were chosen for their computational efficiency since both utilize a transformation filter, which makes the approach appropriate for on-stand testing.

There are many similarities between the inverse TR method and impulse method. In particular, both approaches utilize filter form solutions to transform the internal measurements into surface conditions. However, while the inverse TR method uses a single filter, the impulse response method uses four independent filters in a cascading manner. Both approaches can be applied to a composite system with any number of layers. However, the subsequent formulations presented through this paper focuses on a two-layer system.

1.3.1. Inverse TR method

The present study replicates the work of Najafi et al. [15] and compares this processing to an impulse response filter. This section provides some necessary details to understand the underlying mathematics behind the solution. However, readers are directed to the original study for a full description of the implementation process.

Najafi et al. [15] present a solution to the IHCP for a two-layer medium for which temperatures are known at two internal points. The approach is based on subdividing the domain into two regions and subsequently solving the IHCP for the inner layer through the use of single-layer analytical solutions based on Green's functions. This solution is coupled to the second region by utilizing the results from the inner (substrate) layer as the interface boundary condition for the outer (coating) layer. Finally, the surface conditions are solved using a separate analytical solution for the outer layer.

The inverse TR method presented by Najafi et al. [15] has several advantages. Mainly, this formulation can account for known contact resistances between the layers. Another advantage is that the process minimizes errors based upon a sum-of-squares approach comparing the error between the computed and known temperature values using a TR. However, this minimization necessitates that the knowledge of the end application is known beforehand, which is not always the case. For the present analysis, a single TR parameter was used based on a step change in heat flux at the surface layer. This TR parameter metric provides a representation of how the formulation would be used if the end application was not known or not well understood.

1.3.2. Impulse response method

The impulse response method for conduction problems was first described by Oldfield [2]. The basis of the technique uses discrete deconvolution to derive filter impulse responses of the same length as the data. Although a description of the filter formulation is briefly presented in this paper, implementation strategies are presented by Oldfield. Similar to Najafi et al. [15], the impulse response technique is general to any linear time invariant system. Contrary to the inverse TR approach, this process does not require any regularization parameters, which simplifies the application of the impulse response filter for a wide range of applications. However, because it is not regularized, the filter is also more prone to instabilities – a potential issue that will be addressed later. Previously, this impulse response method was limited to direct conduction problems [2] or single-layer IHCP solution [18]. The present study uniquely extends its application to multi-layer materials.

Similar to the inverse TR method, the impulse approach splits the problem into two discrete domains. The workflow of the problem is illustrated in Fig. 4. In Fig. 4, the entire gage is subdivided into a substrate and a coating solution. The substrate solution has been detailed previously by Oldfield [2]; it is solved using an elegant superposition of differential and common mode gauges, which bypasses the need to know details of the backing material. These solutions to the differential and common mode gauges are then used to create two filters that correspond to the AC components of T_1 and T_2, respectively. The impulse responses (h_1 and h_2) of those filters are shown in Fig. 4. Applying the filters to the measured temperature traces transforms the data into the heat flux at the interface (q_1).

Table 3
Boundary conditions to a surface step change in heat transfer for a two-layer system.

Boundary Conditions	
$q_0 = -k_1 \frac{\partial T_1}{\partial x} = Q$	at $x = 0$, $t > 0$
$T_c = T_s$	at $x = d_c$
$k_c \frac{\partial T_c}{\partial x} = k_s \frac{\partial T_s}{\partial x}$	at $x = d_c$
$T_s = 0$	at $x \to \infty$

The interface conditions can then be used with the coating solution to obtain the surface conditions, T_0. This second solution step extends the capacities from Oldfield's direct method to an IHCP solution. To create an impulse response filter for the coating solution, an analytical relationship between q_0 and q_1 for a step change in q_1 must be known such that

$$q_0[n] = h[n] * q_1[n] = \sum_{i=0}^{N} h_i q_1[n-i] = h_0 q_1[n] + h_1 q_1[n-1] \ldots . h_N q_1[n-N] \quad (9)$$

where h is the impulse response of the filter. Eq. (9) shows that the impulse response, h can be obtained if a discrete relation between q_0 and q_1 is known. The analytical relationship between q_0 and q_1 was determined using a Laplace transform of Eqs. (1) and (2) with the boundary conditions listed in Table 3.

Eq. (10) displays the response of q_1 for a step change in surface heat flux ($q_0 = Q$) such that

$$\frac{q_1}{q_0} = \frac{q_1}{Q} = \left[\operatorname{erfc}\left(t^{*-1}\right) - \sum_{n=1}^{\infty} A^n \left(\operatorname{erfc}\left(\frac{2n-1}{t^*} \right) - \operatorname{erfc}\left(\frac{2n+1}{t^*} \right) \right) \right] \quad (10)$$

where

$$A = \frac{1-\sigma}{1+\sigma} \quad (11)$$

and the nondimensional temperature (t^*) is

$$t^* = \frac{2\sqrt{\alpha_c t}}{d_c} \quad (12)$$

Fig. 5(a) plots the ratio of the output to the input in Eq. (10) for $\sigma = 1$ across a range of t^* values from 0 to 3 with the normalized input plotted as a dashed line. In Fig. 5(a), there exists a region $t^* \leq 0.4$ for which insufficient nondimensional time is available for the surface step change in heat flux to propagate to the interfacial plane (see Fig. 1). In this region (denoted by the shift), the impulse response of the filter will be infinite because $q_1 = 0$ while $q_0 = 1$. Therefore, to correct the output, the q_1 sequence is shifted and accounted for after the creation of the filter. In practice, this shift represents the first stable filter to transform from q_1 to q_0. This shift is an artifact of the discretization of the temperature data and therefore not an arbitrary regularization parameter.

Fig. 5(b) displays three discrete σ values ranging from 0.1 to 10, illustrating relative insensitivity of the nondimensional shift to this parameter. Although a two-layer system is used in this analysis, this process can be repeated for additional layers that are present, making a more general n-layer solution.

After the "coating solution" heat flux filter is created, a separate "coating solution" temperature filter is used to transform the surface heat flux to the surface temperature. This step is accomplished using a solution presented in Doorly et al. [19] for a two-layer system following the same procedure that was previously described

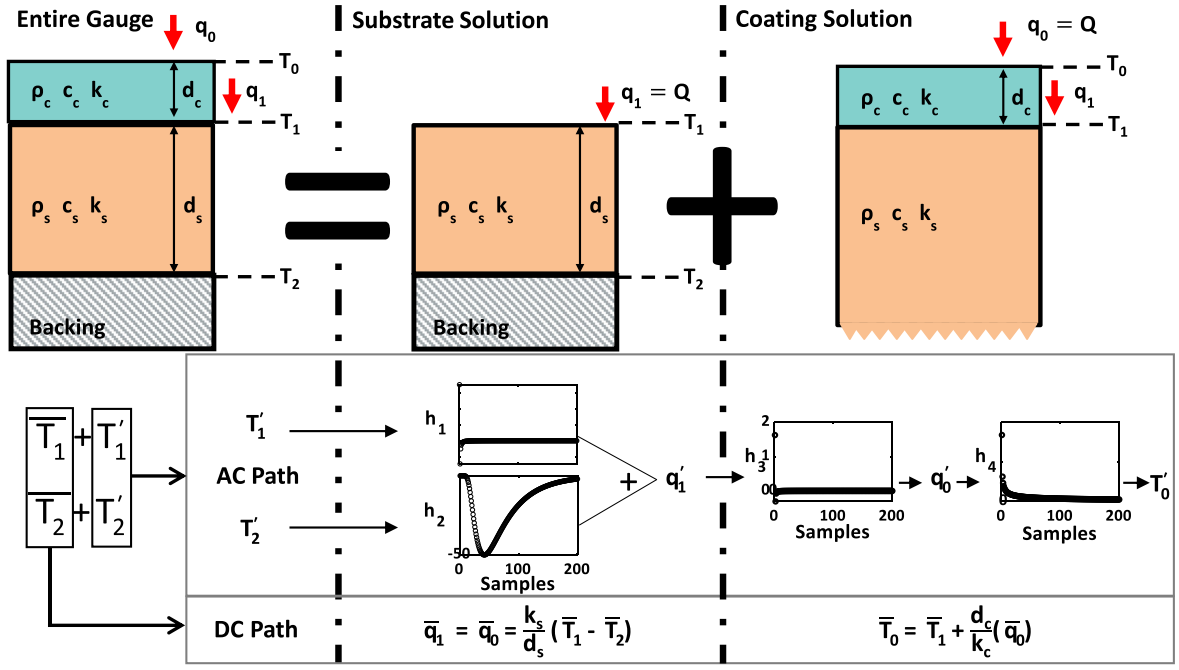

Fig. 4. Implementation work flow for the impulse response method of deducing surface conditions from internal temperature measurements in composite systems.

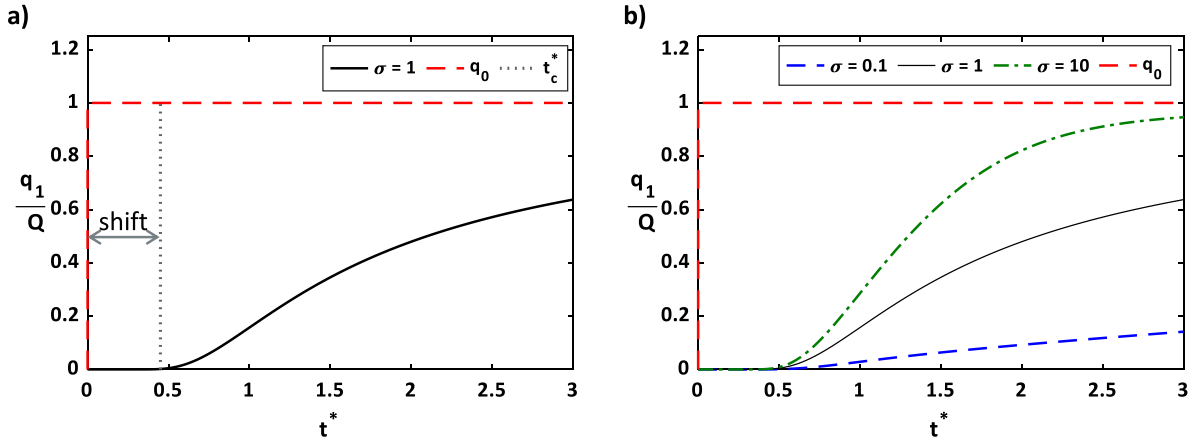

Fig. 5. Solution to the ratio of interfacial heat flux to surface heat flux for (a) $\sigma = 1$, note the shift required to obtain a finite impulse response and (b) three distinct σ values.

above. Importantly, the temperature cannot be independent of the calculated heat flux since only one boundary condition can be imposed at any given time on one boundary.

Fig. 4 also illustrates that the AC and DC path are separated for the proposed analysis. The DC heat flux value depends only on the thickness of the substrate layer (d_s) and the thermal conductivity of the same layer (k_s). A simple 1D conduction network can be used to solve for those parameters. On the other hand, the AC components require the most intensive processing. Separating the time-resolved components from the mean avoids settling times [20] from the impulse response method which implicitly assumes the solution starts at a zero condition. This separation also avoids propagation of mean-value errors and associated concerns with the time-resolved processing.

For large datasets, the impulse and inverse filter require significant time (on the order of hours) to create the necessary filters. However, after the initial computational investment to create the filters, they can be applied relatively quickly. For example, the impulse filters were able to process 1.5 million temperature points in ~1.5 s on a standard desktop computer. In comparison, the inverse TR method was able to process the same data set in ~0.5 s. For this example, the computational time required is negligible; however, this consideration should be taken into account when choosing the appropriate processing scheme for a specific application.

2. Results and discussion

In this section, the previously described methods are utilized to quantify associated errors in the parameters of interest. These two methods are then compared to one another in terms of the error in surface heat flux. After, the impulse method is further explored to determine the process sensitivity of signal noise as well as the geometric and thermal properties of the coating and substrate.

2.1. Comparison of inverse methods

Once the filters for both of these methods were developed, the harmonic solution to the two-layer unsteady conduction equation – Eqs. (3) and (4)–was used as a test case for the processing. These solutions allow idealized analytical temperature traces for

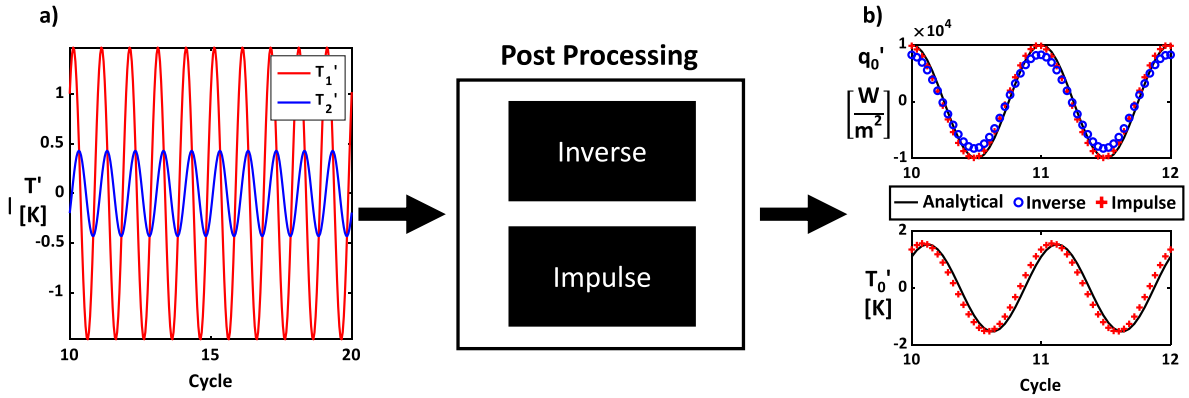

Fig. 6. (a) ideal temperature traces from the analytical conduction solution and (b) corrected signals for the two post processing schemes plotted with the analytical solution.

T_1 and T_2 to be processed through both the inverse TR method as well as the impulse method. The harmonic equation was chosen as the test case because it allows the heating frequency to be varied which can be used to quantify the accuracy of the processing schemes across a broad spectral range. This characterization is important to applications that have numerous important frequencies present simultaneously, such as gas turbine engines [21].

Fig. 6 serves as an example of this comparative processing assessment. Fig. 6(a) uses Eqs. (3) and (4) to create the test traces, T_1 and T_2, respectively. For each case, 50 cycles were simulated with a time step that was sufficiently low to avoid attenuation of the signal. With this definition, the cycles from 10 to 20 were processed using both previously described methods. Fig. 6(b) shows an example of the processed surface temperature and heat flux compared to the analytical solution. In Fig. 6(b), the analytical solution is shown as a solid line, the inverse method is plotted as circles, and the impulse method is plotted as crosses.

These two processing schemes were then characterized in terms of an amplitude error, ϵ_{amp}, given in Eq. (11) as the relative difference between the computational processing and analytical solution such that

$$\epsilon_{amp} = \left| \frac{\hat{X}_{com} - \hat{X}_{an}}{\hat{X}_{an}} \right| \tag{11}$$

where X is a quantity of interest such as surface temperature or heat flux. Following this convention, a phase error, ϵ_{phase}, is also defined as the phase shift between the analytical and computational traces. A discrete Fourier transform was utilized to quantify the ϵ_{amp}, and ϵ_{phase} for each processing scheme [22].

Finally, the results were plotted across all test cases as shown in Fig. 7 where d_c/λ_c was varied from 1×10^{-3} to 10 while σ was held constant at 1.23. This specific σ value corresponds to sensors developed for testing through the current study with a polyimide substrate and Parylene coating. From the impulse response method, several quantities are plotted including the amplitude error (ϵ_{amp}) with respect the analytical solution in q_1, q_0, and T_0 plotted in solid lines. Additionally, the q_0 amplitude error for the inverse TR method is plotted with respect the analytical solution in dashed lines.

Several important processing characteristics are quantified through Fig. 7(a). First, the q_1 amplitude error illustrates the effective errors if the coating is not accounted for in the analysis. This quantifies the interface heat flux error with respect to the analytical surface conditions. These errors correspond to the defined regions in Fig. 3. When $d_c/\lambda_c < 10^{-2}$, the coating is thermally transparent and negligible errors are present in the calculated amplitude. Amplitude errors then increase with d_c/λ_c as the coating increasingly damps the signal, solidifying the need to have a processing scheme capable of capturing the physics of a multi-layer system. When the signal is completely damped, the error in the amplitude reaches a value of unity meaning that insufficient information is available from the damped signal.

The processing necessary to obtain the q_0 and T_0 impulse methods accounts for the coating on the top of the gage surface. Accordingly, q_0 and T_0 impulse methods decrease the error when $d_c/\lambda_c < 3$ compared to q_1. This lower error validates that indirect processing solutions are necessary to avoid excessive errors in that region. However, when $d_c/\lambda_c > 3$, the internal temperature traces are mostly damped and therefore cannot be used to deduce surface quantities. In this region, the impulse response method tends to become unstable, setting a hard cutoff for the usefulness of the processing scheme that corresponds to the physics outlined in previous sections. Fig. 7(b) is a subset of Fig. 7(a) showing errors from $d_c/\lambda_c = 10^{-3}$ to $d_c/\lambda_c = 3$ for the surface quantities using the impulse response method. In this range, the errors were at most 3.2% and were typically below 1%.

The inverse TR method shows a region of increased amplitude error when comparing the q_0 results to the inverse TR method where $10^{-2} \leq d_c/\lambda_c \leq 0.2$. This increase in amplitude error is due to the regularization scheme used to create the inverse TR method which was the least-error-square-fit to a step change in heat flux, not a harmonic solution. However, the identified discrepancy solidifies the conclusion that if experimental conditions are unknown, selection of a regularization scheme is challenging, and the impulse response method is therefore a better processing choice. Note that this comparison between the inverse TR and the impulse methods focuses on the surface heat flux which is more difficult to calculate than the surface temperature [5]. A full characterization of the inverse TR method has been previously presented by Najafi et al. [15] detailing the heat flux and dependent temperature errors associated with the technique.

In addition to the amplitude errors evaluated in Fig. 7, phase errors can also arise from these processing techniques. Phase errors can lead to erroneous interpretation of time resolved-data, especially when synchronizing data across multiple sensors or data acquisition systems. Therefore, it is imperative to quantify the phase error associated with the processing methods. To this end, Fig. 8 quantifies the associated phase errors following the same line styles as outlined in Fig. 7.

The inverse TR method shows similar phase errors in Fig. 8 compared to the impulse method when comparing the q_0 values from $d_c/\lambda_c = 10^{-2}$ to $d_c/\lambda_c = 3$. At $d_c/\lambda_c = 10^{-3}$, there is a slight advantage to the inverse method over the impulse method (on the order of 5°). This discrepancy at lower coating thicknesses

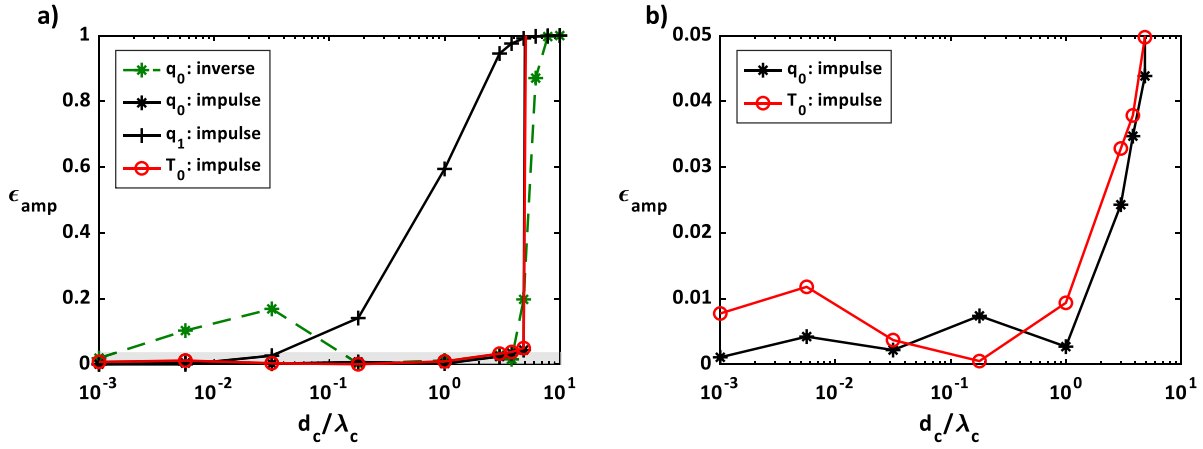

Fig. 7. (a) Amplitude error quantification for surface and internal quantities through both impulse and inverse methods and, (b) gray boxed region in Fig. 7 (a) surface quantities amplitude error for the impulse method where $\sigma = 1.23$.

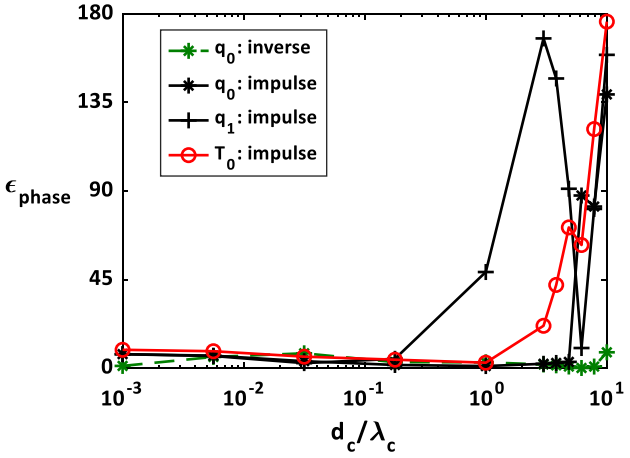

Fig. 8. Phase error quantification for surface and internal quantities through both impulse and inverse methods.

is due to the association of phase error with the impulse method is dependent upon the discretization of the shift in Fig. 5. To accurately capture this shift, relatively high sampling frequencies are necessary. Because the sample rate in this procedure is set by the harmonic heat flux boundary condition, at low d_c/λ_c values, the shift is not adequately captured leading to increased phase errors. This identified error can be mitigated in practice by ensuring the rate of acquisition is sufficiently high to capture the shift highlighted in Fig. 5(a) meeting the criterion in Eq. (12) such that the sample rate, f_s

$$f_s \geq \frac{4\alpha_c}{t_c^{*2} d_c^2} \tag{12}$$

where t^*_c is the critical nondimensional time usually equal to 0.4 with a weak dependency on the σ values.

Overall, both the inverse and impulse show merit in different ways. The inverse TR approach provides a method by which to correctly capture phase at the expense of amplitude errors, whereas the impulse response method does not require a user-selected regularization parameter which is optimal for cases where no prior heat transfer information is known. Because the inverse TR method is well-characterized through other literature, the remainder of this analysis will focus on the impulse method.

2.2. Impulse response processing scheme sensitivities

The previously established processing techniques depend on the geometric and thermal parameters of the system as well as the signal integrity from the temperature measurement devices. Up to this point in the current study, the system has been represented as ideal signals with a perfect knowledge of thermal and geometric parameters. However, in application, signal noise and uncertainty in geometric conditions can both contribute to additional errors. Therefore, this section outlines the sensitivity to those practical factors.

2.2.1. Sensitivity to signal noise

One of the drivers of heat flux uncertainty is amplification of random noise in the temperature signals propagating erroneously as temperature fluctuations through the processing of T_1 and T_2 surface quantities [5]. Traditionally, this phenomenon has been most prevalent at high frequencies where larger amplifications are necessary to deduce heat flux.

In a composite structure, the coating layer acts as an analog filter to the temperature measurement devices below the surface. Knowledge of the configuration can be used to create lowpass digital filters that utilize the physical characteristics of the coating layer(s) to define a cutoff for the possible thermal frequencies (avoiding unwanted electrical noise). To demonstrate this approach, Fig. 9 presents the internal temperature amplitudes normalized by the surface temperature amplitude. For this exercise, a value of $\sigma = 1.23$ was selected for consistency with previous analyses, and associated thermal and geometric properties are based on Table 1. Fig. 9 also displays a horizontal line representing where the amplitude reaches 5% of the surface level values. This cutoff was chosen as the amplitude attenuation where the processing is no longer able to correct the internal temperature traces to surface conditions. The intersection point between the temperature traces and the 5% line defines the cutoff frequency for the lowpass filters.

Digital lowpass filters were created using the cutoff values defined graphically in Fig. 9, and those filters were subsequently implemented using a zero-phase filtering procedure to avoid introducing additional phase errors. These signal filters were tested by adding Gaussian noise at 10% of the maximum amplitude T_1 measurement for a given solution. After adding noise, the signals were filtered and processed, as outlined in the previous sections. The calculated amplitude errors are displayed in Fig. 10.

In Fig. 10, three different q_0 cases were characterized: the ideal signal (characterized previously in Fig. 7), the raw signal with noise, and the filtered signal with noise. The ideal signal demon-

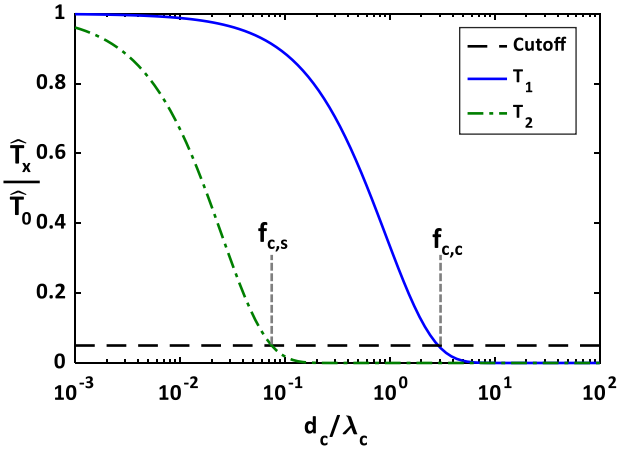

Fig. 9. Internal temperature sensors amplitude with respect to surface temperature amplitude for $\sigma = 1.23$ showing the determination of filter cutoff locations.

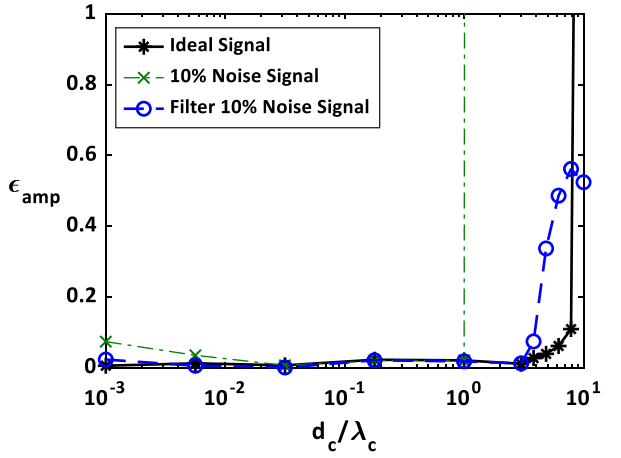

Fig. 10. Amplitude error for impulse response processing under three different noise considerations.

strates the best stability, with minimal errors up to a value of approximately $d_c/\lambda_c = 3$. The addition of noise increased errors at very low d_c/λ_c values – an observation that is expected due to the poor signal to noise ratios. Interestingly, the addition of noise to the signal resulted in minimal error increase for intermediate d_c/λ_c values. This result is due to the fact that the amplitude is being calculated using a discrete Fourier transform which focuses on one specific frequency which is not always affected by gaussian noise. The addition of noise also causes the solutions to become unstable at a $d_c/\lambda_c > 1$, limiting the region of the gage use.

Fig. 10 shows benefits from the addition of lowpass filters. First, the filter extended the stability of the processing region to $d_c/\lambda_c = 3$, which coincides with the T_1 cutoff set in Fig. 9. Second, the quantified amplitude errors were the same as the ideal case with the exception of low d_c/λ_c values because this region is below the cutoffs defined in Fig. 10. Essentially, there is no way to reduce the noise in this region because it cannot be discerned from physical temperature variations.

2.2.2. Sensitivity to geometric and thermal properties

Because thermal and geometric properties are often not perfectly known, it is imperative to understand the sensitivity of those parameters to selected processing schemes. Although these properties are sometimes deduced as lumped parameters (such as k/d) [3,23], the following analysis lists each input property and geometric input separately to show the individual impact of each if measured independently.

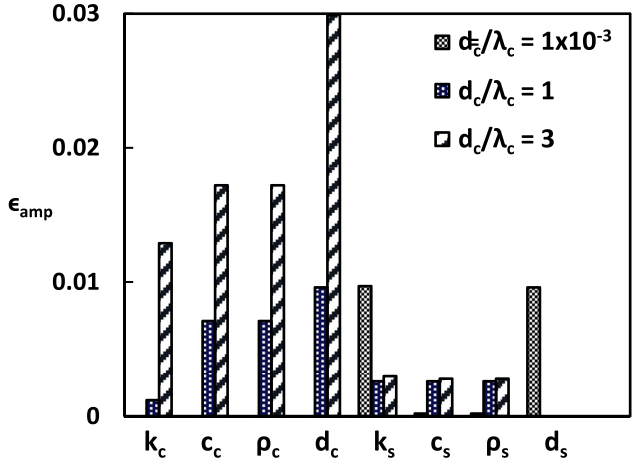

Fig. 11. Sensitivity of q_0 amplitude error to the thermal and geometric properties of the system.

The analysis was conducted through a perturbation method [24] where each parameter was perturbed by 1% of its original value. To calculate the error, the relative change in the amplitude from the perturbed solution was calculated with respect to the normal solution and presented as an absolute value. Fig. 11 shows the results of this analysis for three discrete d_c/λ_c values: 1×10^{-3}, 1, and 3. As with prior sections of the present study, this perturbation analysis was conducted for a nominal case represented by $\sigma = 1.23$.

The results in Fig. 11 are split into three distinct d_c/λ_c values representing the regions outlined in Fig. 3. At low d_c/λ_c values, the system is largely independent of the coating properties itself. This low d_c/λ_c value is similar to a constant heat flux condition where only the thickness (d_s) and the thermal conductivity (k_s) of the substrate are necessary to deduce the heat flux. This is shown in Fig. 11 since the only sources of error at the low d_c/λ_c value were from those parameters.

As the d_c/λ_c values increase, the AC amplitude error from the substrate thickness goes to zero. However, the other substrate and coating parameters begin to affect the results. The substrate parameters (k_s, c_s, and ρ_s) come to discrete, constant values. Previous studies have found that the RMS error in single layer direct problems [3] was related to the thermal effusivity ($\sqrt{\rho_s c_s k_s}$), which explains the error dependence. The coating property sensitivity is less straightforward than the substrate properties. The sensitivity to these parameters changes with the intermediate and high d_c/λ_c values. The most evident example of this increased error is in the d_c value where a 1% error in the thickness could propagate to a 1% error in q_0 at $d_c/\lambda_c = 1$ and a 3% error at $d_c/\lambda_c = 3$.

The sensitivity of the surface heat flux to the coating properties at intermediate and high d_c/λ_c values is still dependent upon the lumped parameters of k_c/d_c and $\sqrt{\rho_c c_c k_c}$, as shown in the previous section. However, the coating material properties only affect the AC component of the surface quantities. An increase in k_c/d_c erroneously increases the amplitude heat flux while an increase in $\sqrt{\rho_c c_c k_c}$ erroneously decreases the amplitude. These competing effects lower the sensitivity to k_c measurements as seen in Fig. 11.

Caution must be taken when using a system of this type to ensure that both the substrate and coating are properly characterized. As shown in this section, even a 1% error in coating thickness could lead to significant errors. To ensure the linearity of the perturbation analysis, a 5% perturbation test was also conducted.

The results were five times the values presented in Fig. 10, building confidence in the linearity of the sensitivity.

3. Conclusions

The study outlines the design considerations for two-layer heat transfer gauges using the solution to the corresponding unsteady conduction equation with harmonic surface heat flux. This analysis uncovers the ratio of coating thickness to thermal wavelength (d_c/λ_c) and the ratio of thermal effusivities (σ) as the driving parameters of the design. These parameters were found to dictate the feasibility of the design by showing that: (1) a system operating at low d_c/λ_c can be treated as a direct problem; (2) a system operating at intermediate values of d_c/λ_c requires a IHCP solution; and (3) a system operating at $d_c/\lambda_c > 3$ exhibits excessive thermal damping making reconstruction of surface conditions infeasible.

This study then addresses the need for novel solutions to the IHCP by proposing an alternative to traditional inverse methods through the impulse method. The impulse method decouples regularization from the inverse solution, and therefore is well-equipped to handle end applications for which the form of the heat flux may not be characterized. When comparing the two approaches, the impulse method showed lower amplitude errors across all tested values of d_c/λ_c at the potential cost of increased phase errors.

When considering real-world factors, such as signal noise, the impulse processing yielded unstable outputs above certain d_c/λ_c values. However, the addition of a digital filter as part of the processing scheme improved stability of the solutions. This filter effectively acts as a regularization to increase processing stability, decoupled from the processing filters themselves. Furthermore, the impulse processing approach was found to be relatively insensitive to errors stemming from uncertainty of thermal and geometric properties. As an exception, the coating properties (particularly the coating thickness) can cause significant errors at large d_c/λ_c values. Therefore, it is important to properly characterize these parameters when employing a gage of this type.

Overall, this study adds to a framework for the design and processing of multi-layer heat transfer gauges with internal temperature measurements. The presented design guidelines will aid in the implementation of surface temperature and heat flux quantification in both new and existing systems in various research and industrial applications. Finally, the impulse processing method offers a new option for this class of inverse problems, enabling user-oriented choices based upon application need.

Declaration of Competing Interest

The authors declare that they have no known competing financial interests or personal relationships that could have appeared to influence the work reported in this paper.

CRediT authorship contribution statement

Shawn Siroka: Methodology, Writing – original draft. **Reid A. Berdanier:** Visualization, Formal analysis. **Karen A. Thole:** Writing – review & editing, Formal analysis.

Acknowledgments

Appreciation is given to Prof. Martin Oldfield who shared the direct versions of the Impulse Response HFG methodology, which were extended to create this work. The authors would like to recognize and thank the U.S. Department of Energy National Energy Technology Laboratory under Award Number DE-FE0025011 for supporting research presented in this paper. This report was prepared as an account of work sponsored by an agency of the United States Government. Neither the United States Government nor any agency thereof, nor any of their employees, makes any warranty, express or implied, or assumes any legal liability or responsibility for the accuracy, completeness, or usefulness of any information, apparatus, product, or process disclosed, or represents that its use would not infringe privately owned rights. Reference herein to any specific commercial product, process, or service by trade name, trademark, manufacturer, or otherwise does not necessarily constitute or imply its endorsement, recommendation, or favoring by the United States Government or any agency thereof. The views and opinions of authors expressed herein do not necessarily state or reflect those of the United States Government or any agency thereof.

References

[1] P.R.N. Childs, J.R. Greenwood, C.A. Long, Heat flux measurement techniques, Proc. Inst. Mech. Eng. Part C J. Mech. Eng. Sci. 213 (7) (1999) 655–677.
[2] M.L.G. Oldfield, Impulse response processing of transient heat transfer gauge signals, J. Turbomach. 130 (2) (2008) 021023 1–9.
[3] A.H. Epstein, G.R. Guenette, R.J.G. Norton, C. Yuzhang, High-frequency response heat-flux gauge, Rev. Sci. Instrum. 57 (4) (1986) 639–649.
[4] T.V. Jones, D.L. Schultz, Heat-transfer measurements in short-duration hypersonic facilities, in: Proceedings of the 4th National UK Heat Transfer Conference, 1973.
[5] J.V. Beck, B. Blackwell, C.R.S. Clair, Inverse Heat Conduction : Ill-Posed Problems, Wiley, New York, 1985.
[6] A.N. Tikhonov, V.Y. Arsenin, Solutions of Ill-Posed Problems, Washington: Winston, New York: Distributed solely by Halsted Press, 1977 V.H. Winston; J. Wiley.
[7] S. Zhao, D. Xia, X. Zhao, A fast image reconstruction method for planar objects ct inspired by differentiation property of fourier transform (DPFT), Inverse Probl. 37 (7) (2021) 075001 1–27.
[8] G.M.L. Gladwell, Inverse problems in vibration, Appl. Mech. Rev. 39 (7) (1986) 1013–1018.
[9] N.M. Al-Najem, Whole time domain solution of inverse heat conduction problem in multi-layer media, Heat Mass Transf. Stoffuebertrag. 33 (3) (1997) 233–240.
[10] K.A. Woodbury, J.V. Beck, Estimation metrics and optimal regularization in a tikhonov digital filter for the inverse heat conduction problem, Int. J. Heat Mass Transf. 62 (1) (2013) 31–39.
[11] J.V. Beck, Filter solutions for the nonlinear inverse heat conduction problem, Inverse Probl. Sci. Eng. 16 (1) (2008) 3–20.
[12] F. Samadi, F. Kowsary, A. Sarchami, Estimation of heat flux imposed on the rake face of a cutting tool: a nonlinear, complex geometry inverse heat conduction case study, Int. Commun. Heat Mass Transf. 39 (2) (2012) 298–303.
[13] J.V. Beck, B. Blackwell, A. Haji-Sheikh, Comparison of some inverse heat conduction methods using experimental data, Int. J. Heat Mass Transf. 39 (17) (1996) 3649–3657.
[14] F. Kowsary, M. Mohammadzaheri, S. Irano, Training based, moving digital filter method for real time heat flux function estimation, Int. Commun. Heat Mass Transf. 33 (10) (2006) 1291–1298.
[15] H. Najafi, K.A. Woodbury, J.V. Beck, A filter based solution for inverse heat conduction problems in multi-layer mediums, Int. J. Heat Mass Transf. 83 (2015) 710–720.
[16] H. Najafi, K.A. Woodbury, J.V. Beck, N.R. Keltner, Real-time heat flux measurement using directional flame thermometer, Appl. Therm. Eng. 86 (2015) 229–237.
[17] G.E. Myers, Analytical Methods in Conduction Heat Transfer, McGraw-Hill, New York, Düsseldorf, 1971.
[18] A.P. Fernandes, M.B. dos Santos, G. Guimarães, An analytical transfer function method to solve inverse heat conduction problems, Appl. Math. Model. 39 (22) (2015) 6897–6914.
[19] J.E. Doorly, M.L.G. Oldfield, The theory of advanced multi-layer thin film heat transfer gauges, Int. J. Heat Mass Transf. 30 (6) (1987) 1159–1168.
[20] S. Siroka, R.A. Berdanier, K.A. Thole, K. Chana, C.W. Haldeman, R.J. Anthony, Comparison of thin film heat flux gauge technologies emphasizing continuous-duration operation, J. Turbomach. 142 (9) (2020) 091001 1–10.
[21] C.H. Sieverding, T. Arts, R. Dénos, J.F. Brouckaert, Measurement techniques for unsteady flows in turbomachines, Exp. Fluids 28 (4) (2000) 285–321.
[22] S Siroka, I Monge-Concepción, RA Berdanier, MD Barringer, KA Thole, C Robak, Correlating Cavity Sealing Effectiveness to Time-Resolved Rim Seal Events in the Presence of Vane Trailing Edge Flow V05BT14A011 (2021) ASME, doi:10.1115/GT2021-59285.
[23] E. Piccini, S.M. Guo, T.V. Jones, The development of a new direct-heat-flux gauge for heat-transfer facilities, Meas. Sci. Technol. 11 (4) (2000) 342–349.
[24] R.J. Moffat, Contributions to the theory of single-sample uncertainty analysis, J. Fluids Eng. 104 (2) (1982) 250–258.